Monomer Capture in Brookhart's Ni(II) Diimine Olefin Polymerization Catalyst: Static and Dynamic Quantum Mechanics/Molecular Mechanics Study

Tom K. Woo,[†] Peter E. Blöchl,[‡] and Tom Ziegler*,[†]

Department of Chemistry, University of Calgary, 2500 University Drive, NW, T2N1N4, Calgary, Alberta, Canada, and IBM Zurich Research Laborattorium, Säumerstrasse 4, CH-8803 Rüschlikon, Switzerland

Received: July 27, 1999; In Final Form: October 19, 1999

A combination of quantum mechanics and molecular mechanics QM/MM has been used to study the capture of ethylene by Brookhart's Ni diimine catalysts of the type (ArN═C(R′)−C(R′)═NAr)Ni^{II}−propyl$^+$ with (**1**) R′ = H and Ar = H, (**2**) R′ = H and Ar = 2,6-C_6H_3(*i*-Pr)$_2$, or (**3**) R′ = CH_3 and Ar = 2,6-C_6H_3(*i*-Pr)$_2$. The study made use of both conventional "static" density functional theory (DFT) based calculations as well as slow growth first principle molecular dynamics (FPMD) DFT methods to examine the capture of ethylene. Examination of the static potential energy surface of all three catalyst models **1**, **2**, and **3** reveals that there is no enthalpic barrier to the capture process. However, both the static and molecular dynamics simulations suggest that there is an entropic barrier to the association that originates from the loss of rotational and translational entropies upon association. The FPMD QM/MM slow growth barriers were calculated to be 7.5, 10.3, and 10.8 kcal/mol at 300 K for catalysts **1**, **2**, and **3**, respectively. An analysis suggests that the trend in the barriers can be related to the size of the active site. The free energy barrier for the pure QM model of **1** has also been estimated from a series of frequency calculations. This approach provides a barrier of 7.7 kcal/mol (and 6.8 kcal/mol without quantum dynamical contributions), which is in fair agreement with the 7.5 kcal/mol barrier (without quantum dynamical contributions) calculated from the slow growth simulations. Analysis of the estimate from the frequency calculations suggests that this barrier estimate represents an upper limit, since the components of the vibrational entropy that compensate the loss of rotational and translational entropy upon association are partially neglected in the treatment.

1. Introduction

There have been an abundant number of computational studies of olefin polymerization catalysts including pure molecular mechanics studies,[1−5] conventional electronic structure calculations,[6,7] and most recently, Car−Parrinello molecular dynamics (MD)[8] and combined quantum mechanics and molecular mechanics (QM/MM) simulations.[9] Virtually all of the theoretical studies have focused on the insertion and chain termination processes. One part of the chain propagation that has been overlooked to some degree in theoretical (and experimental) studies is the monomer capture process. The reason for this is that the capture of the monomer is not considered to be the rate-determining step under normal polymerization conditions.[10] The specific case of Brookhart's Ni(II) olefin polymerization catalyst[11] is unique in that the capture process is believed to play an integral role in controlling the chain branching.

Also, the reverse of the capture process, the monomer ejection, has been neglected, although it plays a role in the chain termination. In most single-site catalytic systems, β-hydrogen elimination has been experimentally implicated to be the dominant chain termination process.[10] Whether the β-elimination process is a unimolecular β-hydrogen transfer to the metal (not shown) or a bimolecular β-H transfer to the monomer (Figure 1), the process is not completed until the olefin terminated polymer chain is ejected. The rate-determining step has been assumed to be the hydrogen-transfer process and not the ejection of the π-bound polymer chain. As depicted in Figure 1, the ejection of the polymer chain can occur in a purely dissociative manner or by the associative displacement by the monomer. Detailed theoretical studies of the termination process generally neglect the ejection process even though the olefin binding energies are often calculated to be in excess of 30 kcal/mol. Although there is an entropic cost to association that offsets the strong enthalpic tendency for olefin complexation, this has a limiting value of 12−15 kcal/mol ($T\Delta S°$ at 298 K) for typical sized catalyst systems.[12] Thus, in some cases the ejection of the chain may in fact be the rate-limiting process and not the hydrogen transfer. We shall in the present study investigate the free energy surface for both the olefin capture and the olefin elimination in Brookhart's Ni(II) olefin polymerization catalyst, (ArN═C(R′)−C(R′)═NAr)Ni^{II}−R^+, as an extension of a previous study in which we explored the influence of the R′ substituent on the enthalpy of olefin capture/elimination.[13]

The free energy of the olefin capture/ejection process can be mapped out by performing a series of frequency calculations on the static potential energy surface. Since these are computationally expensive calculations, even with density functional methods, these calculations are sparse. Furthermore, only the free energies of the overall capture process have been examined in this way.[14] To date no one has examined the "whole" free energy profile of the capture/ejection process to determine if there is a barrier to the process. The mapping of the entire free energy profile of the capture is hampered by the fact that the free energy transition is likely to lie in the weak bonding regime where there may be difficulties in applying a frequency calculation.[15] Furthermore, since the process has a large entropic contribution, the maximum on the zero-temperature energy surface is not likely to match the position of the free energy

[†] University of Calgary.
[‡] IBM Zurich Research Laborattorium.

10.1021/jp992607b CCC: $19.00
Published on Web 12/09/1999

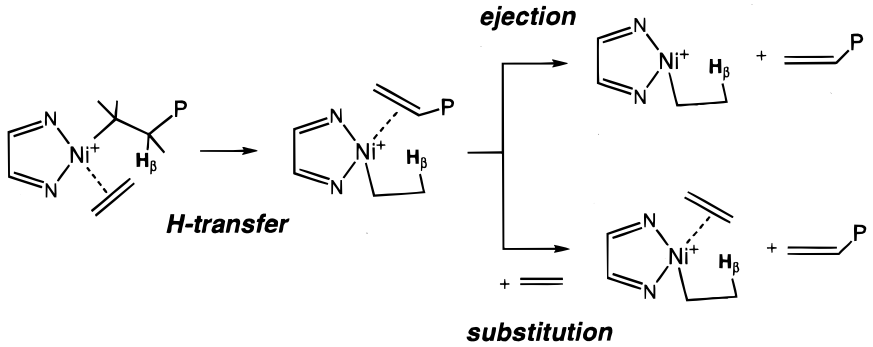

Figure 1. Full chain termination process including the loss of the olefin-terminated polymer chain.

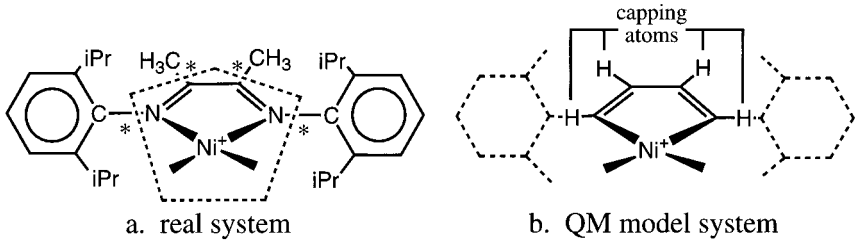

Figure 2. QM/MM partitioning of the Ni diimine catalyst (ArN=C(CH_3)−C(CH_3)=NAr)Ni−R^+ used in this study: (a) so-called "real system" where the link bonds are labeled with asterisks; (b) QM model.

transition state. Thus, a number of expensive frequency calculations along the surface would be necessary to locate the maximum on the free energy surface. Finally, this is all further complicated when considering the process in solution where entropies of molecules are subject to more uncertainties.[16] An alternative to the static approach to examining the free energy profile of the process is to use molecular dynamics or Monte Carlo methods. Here, the PAW QM/MM method provides us with a unique tool to explore the process.

In this investigation we map out the free energy surface of the monomer capture process for Brookhart's Ni(II) olefin polymerization catalyst, (ArN=C(R′)−C(R′)=NAr)Ni^{II}−R^+ using a combination of static and dynamic methodologies. Our previous QM/MM calculations[9a] revealed that there was no enthalpic capture barrier for the Ar = 2,6-C_6H_3(*i*-Pr)$_2$, R′ = CH_3 catalyst system. However, the existence of a free energy barrier cannot be precluded. If a significant free energy barrier exists, then this may have possible implications to the chain termination and branching processes.

2. Computational Details

For the model QM system **1** (ArN=C(R)−C(R)=NAr)Ni−X^+; Ar = R = H) all static DFT calculations were carried out by the Amsterdam density functional program package ADF.[17] The electronic configurations of the molecular systems were described by a triple-ζ basis set on nickel[18] for 3s, 3p, 3d, 4s, and 4p. Double-ζ STO basis sets were used for carbon (2s, 2p), hydrogen (1s), and nitrogen (2s, 2p), augmented with a single 3d polarization function except for hydrogen where a 2p function was used. The $1s^22s^22p^6$ configuration on nickel and the $1s^2$ shell on carbon and nitrogen were assigned to the core and treated within the frozen core approximation. A set of auxiliary[18c] s, p, d, f, and g STO functions centered on all nuclei was used in order to fit the molecular density and present Coulomb and exchange potentials accurately in each SCF cycle. Energy differences were calculated by augmenting the local exchange−correlation potential by Vosko[19] et al. with Becke's[20] nonlocal exchange corrections and Perdew's[21] nonlocal correlation correction. Geometries were optimized including nonlocal corrections. First-order scalar relativistic corrections[22] were added to the total energy, since a perturbative relativistic approach is sufficient for 3d metals. In view of the fact that all systems investigated in this work show a large HOMO−LUMO gap, a spin-restricted formalism was used for all calculations.

All stationary points for the real species **2** (2,6-C_6H_3(*i*-Pr)$_2$)N=C(H)−C(H)=N(2,6-C_6H_3(*i*-Pr)$_2$))Ni−X^+ and **3** (2,6-C_6H_3(*i*-Pr)$_2$)N=C(CH_3)−C(CH_3)=N(2,6-C_6H_3(*i*-Pr)$_2$))Ni−X^+ have been optimized with the ADF QM/MM program using a modified version[23] of the original IMOMM coupling scheme of Maseras and Morokuma.[24] Figure 2 depicts the QM/MM partitioning of the full Ni diimine catalyst **3**. Carbon atoms in Figure 2 labeled with asterisks represent the MM-link atoms at the QM/MM boundary. Use has been made of a link bond ratio,[23] α, of 1.385 for the N−C(aryl) link bond in order to reproduce the average bond distance of 1.44 Å observed in related experimental X-ray crystal structures.[25]

An augmented AMBER95 force field[26] was utilized to describe the molecular mechanics potential. When the AMBER atom type labels as described in the litterature[26] were employed, the diimine carbon was assigned with atom type "CM" parameters, the diimine N with "N2", the aryl ring carbon atoms with "CA", the aryl ring hydrogen atoms with "HA", and the remaining carbon and hydrogen atoms of the MM region with "CT" and "HC", respectively. For the propagation and termination processes, the reacting ethene monomer was assigned with sp^2 "C" van der Waals parameters through to the transition state structure and changed to sp^3 "CT" parameters in the product. A similar procedure was followed for the isomerization process. Alkyl carbon and hydrogen atoms of the active site were assigned "CT" and "HC" van der Waals parameters, respectively. Ni was assigned the "Ni 4 + 2" van der Waals parameters of Rappé's UFF.[27] Electrostatic interactions were not included in the molecular mechanics potential.

In this study, structural optimization of the QM/MM complexes involved a global minimum search of the MM subsystem[13b] with the QM subsystem frozen.[13] The global minimum search involved performing 100 ps of molecular dynamics on the MM subsystem at 800 K where structures were sampled every 2 ps.

Each of the 50 sampled structures was then partially optimized. The best 10 of these partially optimized structures was then fully optimized. The resulting lowest energy structure was considered to be the "global" minimum for the particular frozen QM geometry. During the full optimization of the QM/MM system, the global minimum search was performed once at the beginning to provide the "best" initial MM structure for the given QM structure. The global search was not used in subsequent geometry optimization cycles. However, upon convergence of the geometry optimization, the global search was repeated in order to ensure that a new global MM minimum did not evolve as the QM subsystem changed. If the resulting structure was found to be more stable than the original by 0.2 kcal/mol, then the whole QM/MM optimization process was repeated starting from this new structure.

Ethene binding energies were calculated as the total energy of the olefin π-complex subtracted from the total energy of the free metal alkyl complex plus the free ethene. For all complexes, the growing chain was modeled by a propyl group. The propyl group has been previously shown[8a] to be an appropriate model for the growing chain, since it accounts for the β- and γ-agostic interactions with the metal center.

For the static linear transit ADF calculations reported, all degrees of freedom were optimized except for the reported reaction coordinate. Both forward and backward scans were performed within the critical sections of the potential energy surface (i.e., stationary points or similar). QM/MM frequency calculations were performed using a method described elsewhere.[13a] With QM/MM and pure QM frequency calculations, a two-point numerical differential of the energy gradient was performed in order to determine the Hessian matrix. Thermodynamic properties were evaluated according to standard textbook procedures.[28a,b] Since the vibrational entropy computed from the harmonic frequencies is extremely sensitive to variations in frequencies under 200 cm^{-1}, it is recommended practice to replace the harmonic approximation for low-lying modes with a more realistic expansion of the potential surface.[28b] However, in the present case the low-lying modes involved cannot be described within one of the well-known approximations such as the hinder-rotor model. Unless otherwise specified, modes under 50 cm^{-1} have been removed from the analysis, the default setting in ADF. We estimate errors in our relative free energy calculations due to this approximation to be ± 4 kcal/mol for $T\Delta S_{vib}$, ± 1.2 kcal/mol for ΔH_{zpe}, and ± 0.5 for ΔH_{vib} at 298 K. The error bars were estimated by examining the variation in these properties as a function of the cutoff used in our frequency analysis.

All reported molecular dynamics simulations were carried out with the Car−Parrinello[29] projector augmented wave (CP-PAW) code developed by Blöchl[30] and extended by Woo et al.[9b] to combine quantum mechanics and molecular mechanics (CP-PAW-QM/MM). The density functionals, QM/MM partitioning (Figure 2) and MM force fields employed for the QM/MM-ADF calculations, were used in the CP-PAW-QM/MM simulations as well.

The molecular mechanics region was oversampled by a 20:1 ratio over the QM region[236] to enhance the sampling of the large and "floppy" aryl rings. Time steps of 7 and 7/20 au were used for the QM and MM subsystems, respectively. Masses of the nuclei were set to 50.0 amu for Ni, 2.0 amu for N and C, and 1.5 amu for H in the QM region (including the MM link atoms). MM atoms directly bonded to the MM link atoms were rescaled 10-fold such that the masses of hydrogen and carbon were 0.15 and 0.2 amu, respectively. The masses of all other MM nuclei were rescaled 400-fold to 0.005 amu for carbon and 0.00375 amu for hydrogen. Since we do not discuss time-dependent properties and since configurational ensemble averages remain unchanged under a rescaling of the masses, this technique is appropriate. Unless otherwise specified, the electronic structure calculation of the QM model system involved a unit cell spanned by the lattice vectors ([0.0 9.5 9.5][9.5 0.0 9.5][9.5 9.5 0.0]). Separate thermostats were used for the QM and MM regions.

The free energy barriers were calculated using the "slow growth" technique, which has been detailed and demonstrated on other olefin polymerization catalysts.[8a−d] With the slow growth technique, a reaction coordinate (RC) is constrained during the dynamics and slowly varied from a value characteristic of the initial state to a value characteristic of the final state of interest. The Helmholtz free energy difference ΔF between two arbitrary points $\lambda = 0$ and $\lambda = 1$ along the RC is determined as

$$\Delta F = \int_0^1 \left\langle \frac{\partial E}{\partial \lambda} \right\rangle_{\lambda,T} d\lambda \qquad (1)$$

where the number of samples at each point λ equals 1 in the slow growth limit. The slow growth reaction coordinate used in all simulations was the Ni−olefin carbon midpoint distance. In the simulations that are presented here, the total scan time chosen was about 39 000 time steps for each direction.

The PAW QM/MM simulations sample from the *NVT* ensemble and therefore the profiles correspond to Helmhotz free energies. We use ΔF to refer to the Helmholtz free energy determined from the PAW simulations. The frequency calculations correspond to Gibbs free energies, ΔG, at 1 atm constant pressure. In the vacuum, gas-phase limit, the Helmholtz and Gibbs free energies are equivalent, and therefore, the constant pressure correction can be added to our PAW free energies to compare to the corresponding Gibbs free energies of the frequency calculations.

3. Results and Discussion

We have examined the free energy surface of the capture process for three variations of the Brookhart Ni diimine catalyst, (ArN═C(R′)−C(R′)═NAr)Ni^{II}−propyl$^+$. The first catalyst model **1** lacks any of the bulky substituents such that Ar = H and R′ = H. For the last two catalyst models **2** and **3**, the bulky aryl rings Ar = 2,6-C_6H_3(*i*-Pr)$_2$ are modeled by a MM potential. With catalyst model **2** R′ = H, while for **3** the R′ = CH_3 group is also partitioned to the MM region. In all three cases, the electronic structure calculation is performed on the same model system where Ar = H and R′ = H.

Static Capture Profiles. We first examine the "static" potential energy surface of the olefin capture process. In our previous pure QM and QM/MM studies of the Brookhart Ni diimine catalyst, it was noted[9a] that no ethalpic barrier to the capture process could be located. Here, we present a more detailed examination of the potential energy surface in order to relate it to the free energy surface. Figure 3 shows the calculated enthalpy profiles of the ethene capture process for catalyst models **1**−**3**. The profiles were determined from a series of static linear transit calculations where the reaction coordinate is defined as the distance between the midpoint of the olefin double bond and the metal center. The energies plotted are relative to that when the Ni−olefin midpoint distance is 7.0 Å.

Without the influence of the bulky aryl rings, olefin capture in **1** shows a gradual stabilization of the complex as the olefin approaches the metal center. The long-range stabilization is due to the favorable electrostatic interactions of the electropositive

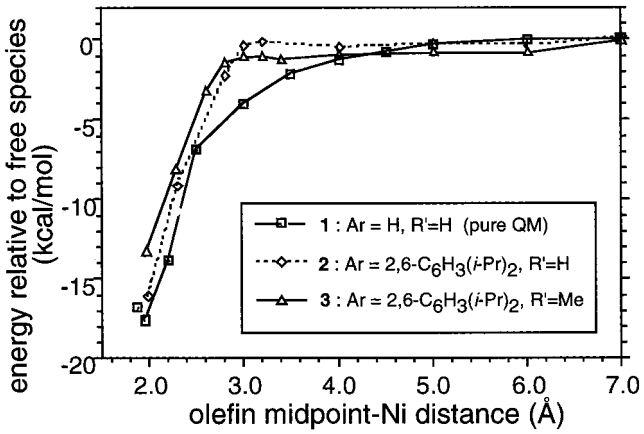

Figure 3. "Static" linear transit energy profiles of the capture process. The reaction coordinate of the linear transit calculations was the distance between the Ni and the midpoint of the olefin double bond. Energies are plotted relative to the stability of the conformations at RC = 7.0 Å.

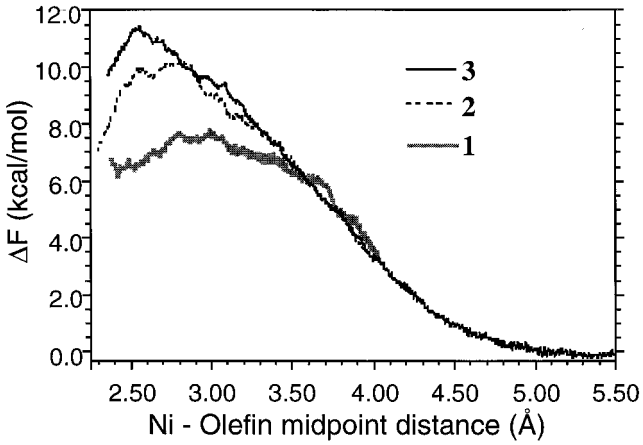

Figure 4. Slow growth free energy profiles of the capture process at 300 K for models **1**−**3**. Free energies are all plotted with the same baseline at a reaction coordinate value of 4.0 Å, where only the profile of **3** is extended.

TABLE 1: Free Energy Barriers Including Hysteresis from Slow Growth Simulations of the Capture Process

structure	description	$\Delta G^{\ddagger}_{\text{capture}}$[a,b] (kcal/mol)	barrier distance[b] (Å)
4	Ar = H, R′ = H	7.5 ± 0.4	2.93 ± 0.05
5	Ar = 2,6-C_6H_3(*i*−Pr)$_2$, R′ = H	10.3 ± 0.2	2.75 ± 0.08
6	Ar = 2,6-C_6H_3(*i*−Pr)$_2$, R′ = CH_3	10.8 ± 0.5	2.66 ± 0.10

[a] Assuming the baseline at a reaction coordinate value of 4.0 Å can be used for all trajectories as discussed in the text. [b] Error bars determined from hysteresis.

metal center and the olefin. The short-range and strong stabilization is attributed to the π-donor−acceptor interactions between the olefin and metal center. In catalyst models **2** and **3** the strong stabilizing interactions are offset by the repulsive steric interactions between the olefin and the aryl rings that force the rings to less favorable perpendicular orientations. Thus, the addition of the bulky rings in the hybrid QM/MM potentials in **2** and **3** produces two notable changes in the capture profiles. First, the exothermicity of the olefin binding decreases as discussed previously.[9a] Second, although there is no clear transition state, there is a plateau with a steep enthalpic cliff leading to the π-complex. The ledge of the plateau occurs at approximately 2.9 Å for **2** and slightly more inward at 2.8 Å for **3**. Again, this can be rationalized in terms of an increased steric hindrance to the formation of the π-complex that delays the net stabilization due to the electronic interaction between the olefin and the metal center.

Slow Growth Free Energy Profiles. To explore the free energy surface of the capture process at 300 K, we have performed a series of molecular dynamics simulations of the process for catalyst models **1**−**3** using the slow growth method. The slow growth reaction coordinate utilized in all simulations was the olefin midpoint to Ni distance. For all three catalyst models, forward and reverse scans were performed where the reaction coordinate was continuously varied from 4.0 to ∼2.3 Å. Plotted in Figure 4 are the resulting free energy profiles of the forward scans (capture). The profiles for all three models are plotted relative to the state at the beginning of the simulation where the reaction coordinate is 4.0 Å. Extension of the profile beyond the RC = 4.0 Å mark was only performed for model **3**, which amounts to 3.5 kcal/mol. The profiles of **2** and **3** are plotted in Figure 4 assuming the same long-range behavior of the free energy profile.

The baseline used in Figure 4 demands some explanation. Extension of the free energy profile beyond the 4.0 Å point is complicated by the fact that the demands of the electronic structure calculation grow with the cell size and at large reaction coordinate values, a relatively large simulation cell is required. For the RC = 2.3−4.0 Å simulation window, the electronic structure calculation is already quite demanding, and extension of the free energy profile for larger reaction coordinate values requires an even larger simulation cell, thereby putting enormous strains on the computational resources. For these reasons, only the free energy profile of **3** was extended beyond the 4.0 Å point. In this extended simulation window a unit cell spanned by the lattice vectors ([0.0 11.5 11.5] [11.5 0.0 11.5] [11.5 11.5 0.0]) in angstroms was utilized. Only the outward scan was performed were the reaction coordinate was varied from 4.0 to 6 Å over 16 000 time steps. At approximately the 5.5 Å mark, the free energy begins to level out where it is 3.4 kcal/mol lower than at the 4.0 Å mark. For all three model systems, the free energy was still dropping at the RC = 4.0 Å mark. However, we note that the slopes of profiles begin to converge at the 3.70 Å point. Comparison of the absolute constraint forces during the simulations reveals that there is also a convergence of the absolute value of the force. This further suggests that in the long-range region, the behavior of the profiles of the three models is similar. This is a reasonable assumption for models **2** and **3**, which have nearly identical structures. However, for model **1**, which does not have the large bulky aryl rings, this assumption is more approximate and the extended profile for this model is likely to drop off more quickly, likely resulting in an overestimation of the barrier in this case.

With the approximation that the same baseline is used for all three model systems for both forward and reverse scans, the slow growth capture barriers are reported in Table 1, with error estimates based on the hysteresis. Also provided in Table 1 are the locations of the free energy maxima in terms of the reaction coordinate. The capture barriers follow the expected trend with **1** < **2** < **3**. Without the bulky aryl rings the capture barrier of **1** lies about 3 kcal/mol lower than that of either **2** or **3**. The free energy barrier of **3**, with R′ = CH_3, is slightly larger than **2** with R′ = H. Since the R′ group is treated in the MM region, the enhanced barrier of **3** is only steric in nature. Our earlier study[13] of the electronic and steric effects of the R′ substituents suggests that the inclusion of electronic effects in model **3** may further enhance the barrier.

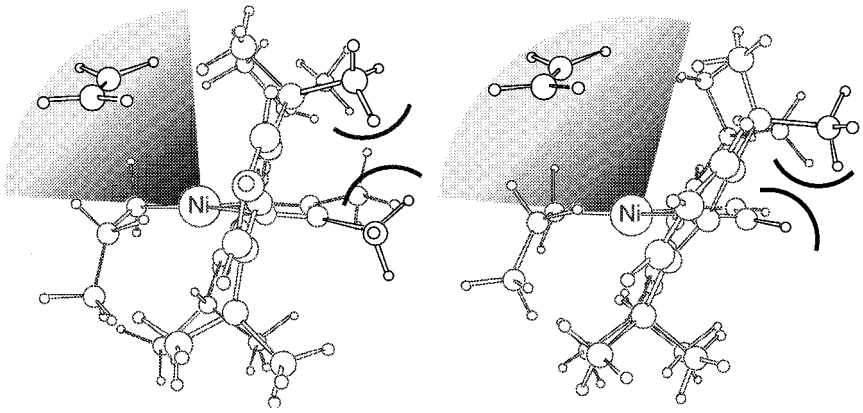

Figure 5. Possible indirect steric effect of the R′ diimine substituents on the monomer capture process.

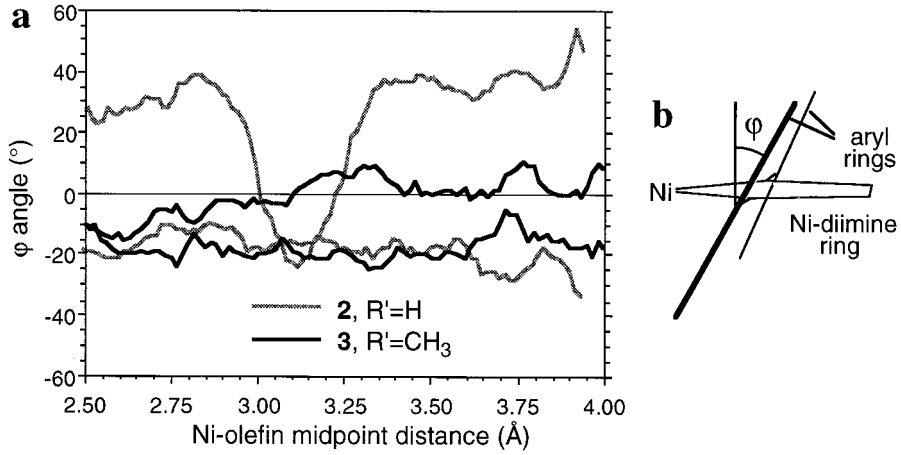

Figure 6. (a) Deviation of the plane angle from perpendicular orientation of the aryl rings relative to the diimine ring extracted from the slow growth simulation of the capture process for models **2** and **3**. (b) Definition of the angle φ.

The location of the free energy maxima also follows the expected trends. As the steric congestion about the metal center increases, the location of the maximum decreases. These trends are in line with the trends observed with the potential "ledges" in our static calculations of the potential surface given in Figure 3. Some other noteworthy observations can be made that relate the free energy profiles with the static potential energy profiles. For example, the gradual slope of the static potential of **1** is translated into a broad free energy barrier. This contrasts with the profiles of **2** and **3**, which have steep enthalpic "ledges" and also steeper behavior of the free energy surface near the maximum. Consistent with the notion that the ethalpic tendency to form the π-complex is offset by entropic factors, the free energy maxima of **2** and **3** lie slightly more inward (∼0.2 Å) than the steep ledges of their respective ethalpic profiles shown in Figure 3. There is one noticeable difference between the "static" profiles and the free energy barriers of Table 1. The olefin capture energies of models **2** and **3** differ by 2.4 kcal/mol, whereas the free energies are approximately the same. Thus, the uptake and capture barriers in this case may be controlled by different factors.

Nature of the Free Energy Barrier. Even without the bulky aryl rings the free energy barrier of capture for model complex **1** is significant, amounting to 7.5 kcal/mol at 300 K according to our slow growth simulations. The slow growth free energy profile of **1** has a maximum at approximately 2.93 Å. At this point the static capture profile of Figure 6 shows that the olefin catalyst complex is only stabilized by 3.5 kcal/mol. If the entropic cost of the association at this point is large, then this could account for the large barriers observed. To further understand the nature of the capture barrier, we have attempted to elicit a free energy barrier of **1** from static frequency calculations. Full ADF frequency calculations of the optimized π-complex and the free alkyl have been performed. Additionally, a constrained frequency calculation has been performed on the linear transit structure at RC = 3.0, approximately where we estimate the free energy maximum to be from the PAW MD simulations. In this frequency calculation the degree of freedom associated with the reaction coordinate is constrained.

TABLE 2: Thermodynamic Data at 298 K for the Olefin Complexation for Model Catalyst 2 Relative to the Free Species

	contribution to $\Delta G°$ (kcal/mol)	
quantity	π-complex	RC = 3.0 Å
$-T\Delta S_{trans}$	+10.6	+10.6
$-T\Delta S_{rot}$	+5.2	+5.1
$-T\Delta S_{vib}$	−3.2	−5.7
$-T\Delta S_{total}$	+12.5	+10.0
ΔH_{trans}	−0.889	−0.889
ΔH_{rot}	−0.889	−0.889
ΔH_{vib}	+1.6	+2.3
ΔH_{ZPE}	+1.6	+0.5
$\Delta E_{complexation}$	−16.9	−3.4
ΔH_{total}	−15.6	−2.3
ΔG at 298 K	−3.1	+7.7

The resulting free energies relative to the free metal alkyl and ethene are reported in Table 2. The free energy of olefin complexation is estimated to be exergonic $\Delta G°_{capture} = -3.1$ kcal/mol at 298.15 K. On the basis of the constrained frequency calculation of the transition-state complex where the reaction

coordinated is fixed to a value of 3.0 Å, the capture barrier is estimated to be 7.7 kcal/mol at 298 K, which is in reasonable agreement with the barrier predicted from the slow growth simulation. (We will discuss the comparison in more detail later.) Table 2 reveals that the entropic cost of association at this point amounts to 10 kcal/mol, whereas the ethalpic stabilization at this point is only 3.4 kcal/mol. Thus, on the basis of this approximation, the capture barrier can be considered to be an entropic barrier resulting in the loss of translational and rotational degrees of freedom upon association.

At this point let us examine the effect of the approximations made in this analysis. We have assumed that the six rotational and translational degrees of freedom are completely converted into vibrational degrees of freedom. When the olefin is weakly bound, the resulting vibrations associated with the olefin metal bond will be of low frequency. Classical statistical thermodynamics[28b] reveals that the absolute vibrational entropy associated with a particular normal mode vibration is inversely proportional to its frequency. Thus, when the olefin is weakly bound, the potentially large loss of rotational and translation entropies is offset because they are transformed into vibrational degrees of freedom with high entropies associated with them. Oppositely, when the olefin is more strongly bound, the vibrations are of higher frequency and therefore have lower absolute entropies associated with them. Thus, the more strongly bound the complex, the higher the entropic cost of association. In general terms, there is an inverse relationship between the exothermicity and the entropic cost of association.[31]

In comparing the relative free energy of the π-complex where the olefin is strongly bound and is the transition-state structure, we notice that the results exhibit this inverse relationship. At the transition-state structure, the enthalpic stabilization amounts to only 3.4 kcal/mol and the $-T\Delta S_{vib}$ compensation is -5.7 kcal/mol. In comparison, at the π-complex where the enthalpic stabilization is about 17 kcal/mol, the compensatory component is diminished to -3.2 kcal/mol. Since all frequencies under 50 cm^{-1} were removed in the thermodynamic analysis, we suggest that the estimated capture free energy barrier of 7.7 kcal/mol provides an upper limit. This is because, in this case, the lowest four vibrational modes were discarded in each calculation, and therefore, potentially four of the six vibrational modes associated with the olefin complexation were removed. Since most of the high entropy vibrational modes that would offset the loss in rotational and translation entropy have been removed from the analysis, we are overestimating the entropic cost of association.

In our treatment we have assumed that the translational and rotational entropies of the interacting components are completely lost and replaced with the vibrational terms. In the limit of no bonding, these vibrational degrees of freedom will become indistinguishable from the lost rotational and translational ones. Thus, it has been suggested that a better approach to treating the entropic cost of weak associations (as in our transition-state structure) is to assume that the translation and rotational entropies of the separate components is not completely lost upon association.[32] In this way, the entropic cost of association is treated as some fraction of the 15.7 kcal/mol maximum ($T\Delta S_{rot} + T\Delta S_{trans}$ of Table 2) that is dependent upon the exothermicity of the association.[16,31] Unfortunately, this approach is also problematic, since there is no satisfactory relationship to determine what fraction to use.

To compare the capture barriers from the static calculations and the molecular dynamics simulations, we must correct the static barrier estimate for terms not accounted for in the MD simulation. The thermodynamic components given in Table 2 that are not accounted for in the PAW slow growth simulation are ΔH_{ZPE}, ΔH_{vib}, ΔH_{trans}, and $\Delta H_{rot.}$.[33] When these components are removed from the static barrier, it drops from 7.7 to 6.8 kcal/mol. This compares to the 7.5 kcal/mol slow growth barrier of the capture process for complex **1**. As discussed before, we suggest that the static barrier estimate represents an upper limit, and thus, it seems that the slow growth method has overestimated the barrier. One possible explanation is that the extended tail of the free energy profile, which was taken from the simulation of **3**, is not exactly the same as for the pure QM model **1**.

The calculated slow growth barrier for the pure QM model **1** was estimated to be 7.5 kcal/mol, whereas for models **2** and **3**, they are 10.3 and 10.8 kcal/mol, respectively. Thus, the addition of the bulky aryl rings increases the barrier by only 3 kcal/mol. Since the barrier is entropic in nature, the difference must arise from the constriction of the active site cavity of the metal center by the aryl rings, which would enhance the loss of rotational and translational entropy of the complexing olefin. From Table 2, we note that for model **2** the entropic cost of association at the transition state is 10 kcal/mol. The same quantity for the π-complex where the olefin is strongly bound is 12.5 kcal/mol, a difference of 2.5 kcal/mol. We would expect that the entropic cost of association at the transition states of **2** and **3** would be somewhere between that of the π-complex and transition state of **1**. With this argument, the difference of 3 kcal/mol observed for the barriers of **2** and **3** with that of **1** is reasonable, albeit somewhat high.[34]

The small but observable barrier difference in capture between models **2** and **3** can be qualitatively rationalized on similar grounds. We suggest that the $R' = CH_3$ substituent in **3** acts to close off the active site due to the interaction with the aryl rings more so than does the $R' = H$ group in **2**. This has been depicted in Figure 5. The openness of the coordination site can be directly related to the angle φ as defined in Figure 6b. The φ angle is related to the plane angle θ except that it measures the angular deviation from the perpendicular orientation of the aryl ring with the central Ni diimine ring as opposed to the deviation from the parallel orientation. Thus, the larger the φ angle, the more open one of the axial coordination sites of the Ni center is, as shown in Figure 5. Plotted in Figure 6b are the φ angles for models **2** and **3** during the course of the slow growth simulation of the capture process. We notice that for complex **3** the φ angles remain under 20° throughout the simulation, whereas in model **2** one of aryl rings has a much larger φ angle. Thus, Figure 6 offers a crude rationalization of the barrier difference as arising from a more adverse entropic cost to association in **3** due to the restriction of the translational and rotational degrees of freedom of the ethene molecule in the more hindered active site compared to that of **2**.

Stability of the Olefin π-Complex. On the basis of experimental NMR studies, the olefin π-complex is believed to be the catalytic resting state with Brookhart's Ni diimine catalyst system.[11] We can estimate the free energy of capture from our molecular dynamics simulations if the trajectory is continued inward until the formation of the π-complex. For model system **3**, for which the free energy surface was mapped outward until it leveled off, a slow growth simulation has been performed where the reaction coordinate has been varied from a value of 1.8 to 2.75 Å over 15 000 time steps. Thus, the entire free energy profile has been mapped out from the olefin π-complex to the "free" species over three simulation windows. The full and piecewise free energy profile is given in Figure 7. Since the outermost slow growth simulation where the reaction coordinate

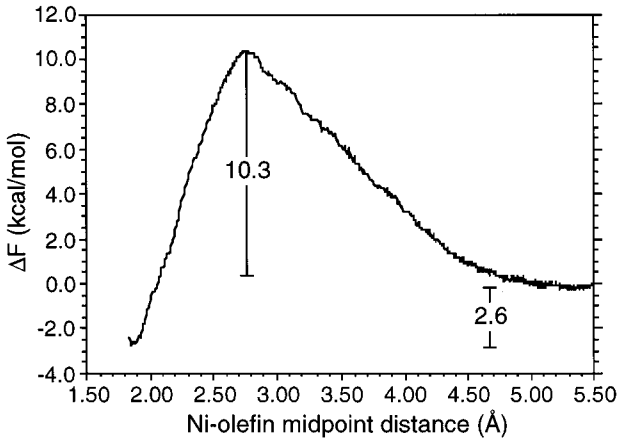

Figure 7. Slow growth free energy profile of the olefin ejection process for model catalyst system **3**. The total profile consists of three separate simulation windows: the innermost window spanning a reaction coordinate range 1.8−2.75 Å, the middle window spanning a range 2.75−4.0 Å, and the outermost window spanning the reaction coordinate values of 4.0−6 Å.

was varied from 4.0 to 6 Å corresponds to the reverse scan, it was decided to also perform the reverse scan of the innermost simulation window from the π-complex to free energy transition state. Thus, plotted in Figure 7 is the full unidirectional slow growth free energy profile of the olefin ejection process from the π-complex outward. The corresponding forward scan of the entire capture process has not been performed because of computational expense of the simulation, particularly for the outermost simulation window.

Figure 7 reveals that the olefin capture is favorable with $\Delta F°_{\text{capture}} = -2.6$ kcal/mol. Thus, the slow growth simulation suggests that (without quantum dynamical effects accounted for) the olefin π-complex is stable in the gas-phase limit at 300 K. This agrees with the experimental observations.[11] This result also agrees with our previous molecular dynamics simulation of the olefin π-complex.[8a] By use of the same methodology,[35] the olefin π-complex of **3** was simulated for 1 ps[36] where no constraint was used to tether the olefin to the metal center. Within this simulation time, the olefin π-complex was found to be stable. This contrasts with previous ab initio molecular dynamics simulations of the zirconocene olefin polymerization catalyst[8a,b] where during simulations of the π-complex it was observed that the olefin would immediately detach itself from the metal center at 300 K if a constraint were not imposed. Interestingly, the catalytic resting state in these complexes is considered to be the free alkyl complex.[10]

We have also estimated the free energy of capture from QM/MM frequency calculations of the free alkyl and the π-complex of **3**. From this we can compare the results from the methods and correct the slow growth estimate for quantum dynamical effects. Table 3 details the various components of the free energy of complexation resulting from this analysis. The entropic cost of association is estimated to be $-T\Delta S = 12.9$ kcal/mol, which is similar to that presented in Table 2 for model catalyst **1** where $-T\Delta S = 12.5$ kcal/mol. The similarity in the results suggests that the free energy of olefin uptake and therefore the equilibrium between the π-complex and metal alkyl is controlled primarily by the ethalpy of binding. The entropic cost of olefin complexation has been measured experimentally by Rix and Brookhart[37] for a similar Pd(II) ethylene−CO copolymerization catalyst and found to be $-T\Delta S = +10.8$ kcal/mol at 300 K. ($\Delta S_{\text{complexation}} = -36$ eu). The agreement between the experimental and theoretical results is fair, but they reaffirm our

TABLE 3: Thermodynamic Data at 298.12 K for the Olefin Complexation for Model Catalyst 3 Based on a QM/MM Frequency Calculation

quantity	contribution to $\Delta G°$ (kcal/mol)
$-T\Delta S_{\text{trans}}$	+10.7
$-T\Delta S_{\text{rot}}$	+5.6
$-T\Delta S_{\text{vib}}$	−3.2
$-T\Delta S_{\text{total}}$	12.9
ΔH_{trans}	−0.889
ΔH_{rot}	−0.889
ΔH_{vib}	+1.8
ΔH_{ZPE}	+2.7
$\Delta E_{\text{complexation}}$	−13.7
ΔH_{total}	11.0
$\Delta G°$ at 298 K	+1.9

analysis that we are overestimating the entropic cost of association in our static calculations. At the same time, the overestimate is not too severe.

The total free energy of olefin complexation is calculated to be endergonic with $\Delta G°_{\text{capture}} = +1.9$ kcal/mol. Thus, in the gas phase our static QM/MM model implies that the olefin π-complex is not stable, which contradicts our molecular dynamics simulations. However, the terms of the static free energy estimate not included in the classical MD simulations amount to +2.7 kcal/mol. When these terms are removed from the static estimation of the free energy, it also becomes negative with $\Delta G° = -0.8$ kcal/mol. Thus, when the free energies are properly compared, there is good agreement. Additionally, as previously stated, we are likely overestimating the entropic cost of association in the static calculations. Thus, when this is considered, the agreement between the static and dynamic calculations improves.

When the quantum effects are corrected in the slow growth estimate of the free energy of capture, the capture becomes endergonic with $\Delta F°_{\text{capture}} = +0.1$ kcal/mol. Thus, both the PAW and the ADF QM/MM estimates of the free energy of complexation are slightly endergonic in the gas phase. This does not agree with the experimental results, which identify the olefin π-complex to be the catalytic resting state. When the electronic effects of the R′ substituents are accounted for,[13] we can expect the estimate of the capture free energy to become even more endergonic. Since these experiments are performed in dichloromethane, the discrepancy between the calculated and experimental results may be due to the solvation. For the low dielectric solvents used for polymerization, we estimate that the effect of solvent upon the free energy of olefin capture will be small. On enthalpic grounds, the solvation will slightly weaken the olefin binding energy. On the basis of continuum solvation calculations using the COSMO[38] implementation within ADF,[39] we predict that the olefin binding energies will diminish by less than 2.7 kcal/mol in dichloromethane.[40] On entropic grounds, the binding will be slightly more favorable in solution, since at standard states the free species have less volume available to them in solution than in the gas-phase. The value of the entropic adjustment can be estimated from the solvent density,[41] and in the case of dichloromethane, it amounts of 3.2 kcal/mol at 300 K. Thus, we suggest that the effect of solvation is to shift the free energy balance toward that of the complexed species.

The results of the static and dynamic calculations are in good agreement with one another. Although the calculated free energies of capture are estimated to be positive, values are close to zero. Aside from sampling errors in the dynamics simulations and the errors due to the low-frequency modes in the normal mode analysis, there is another possible explanation to account

for the calculated positive free energies of complexation. As discussed elsewhere,[13] the so-called indirect steric effect may be overestimated in our QM/MM model because of an overly strong torsional potential used for the N(diimine)−C(aryl) bond.

4. Conclusions

In this section we have attempted to map the free energy surface of the olefin capture and ejection events in the catalytic cycle of olefin polymerization by Brookhart's Ni diimine catalysts of the type (ArN═C(R′)−C(R′)═NAr)Ni^{II}−propyl$^+$. We have used both conventional "static" frequency calculations and slow growth molecular dynamics methods to examine the process for three model catalytic systems. The pure QM model **1** with R′ = H and Ar = H does not possess the bulky aryl rings. In models **2** (R′ = H) and **3** (R′ = CH_3), where Ar═Ar = 2,6-C_6H_3(*i*-Pr)$_2$, the aryl rings and the R′ substituents are accounted for via a molecular mechanics potential. In all three models, the electronic structure calculation involves the (HN═CH−CH═NH)Ni^{II}−propyl$^+$ molecule.

Examination of the static potential energy surface of all three models, **1**−**3**, reveals that there is no enthalpic barrier to the capture process. However, both the static and molecular dynamics simulations suggest that there is an entropic barrier to the association that originates in the loss of rotational and translational entropies upon association that is not compensated by the enthalpy of coordination. The PAW QM/MM slow growth barriers were calculated to be 7.5, 10.3, and 10.8 kcal/mol at 300 K for catalysts **1**, **2** and **3**, respectively. Our analysis suggests that the trend in the barriers can be related to the size of the active site. The more constricted the active site, the greater the loss of entropy before the system can be stabilized by the coordination. From this simple picture the PAW slow growth simulations of the olefin capture exhibit the expected trends in the capture barriers. Catalyst **1** lacks the bulky aryl rings that can block the coordination sites of the metal center, resulting in a 3 kcal/mol smaller barrier than that of either **2** or **3**. The small difference in capture barriers between **2** and **3** can be rationalized in terms of the interaction of the R′ group with the aryl rings that in **3** acts to close off the active site. The free energy barrier for the pure QM model **1** has also been estimated from a series of frequency calculations. This approach provides a barrier of 7.7 kcal/mol (and 6.8 kcal/mol without quantum dynamical contributions), which is in fair agreement with the 7.5 kcal/mol barrier (without quantum dynamical contributions) calculated from the slow growth simulations. Analysis of the estimate from the frequency calculations suggests that this barrier estimate represents an upper limit, since the components of the vibrational entropy that compensate the loss of rotational and translational entropy upon association are partially neglected in the treatment.

We have also examined the stability of the π-complex in the Brookhart catalyst system **3**, which is believed to be the catalytic resting state. The PAW QM/MM slow growth profile of the capture process suggests that the π-complex is more stable than the free metal alkyl and ethene molecule in the gas phase with $\Delta G^\circ_{\text{capture}} = -2.6$ kcal/mol at 300 K. This agrees with our PAW QM/MM dynamics simulation of the π-complex, which reveals that the olefin does not detach within the 1 ps simulation. On the other hand, our ADF QM/MM calculations suggest that the free energy of olefin complexation is positive with $\Delta G^\circ_{\text{capture}} = +1.9$ kcal/mol at 298 K. When quantum corrections are added to the PAW slow growth estimate of the free energy of capture, it also becomes slightly positive, thereby improving the agreement between the two methods. The calculated endergonic gas-phase free energies are in contrast with the experimental result that the olefin π-complex is the catalytic resting state. The discrepancy may be due to solvation effects.

Acknowledgment. This investigation was supported by NSERC of Canada, as well as by the donors of the Petroleum Research Fund, administered by the American Chemical Society (ACS-PRF No 31205-AC3). We thank Drs. P. Margl and L. Deng for useful discussions and Nova Chemicals for support.

References and Notes

(1) Cavallo, L.; Guerra, G.; Oliva, L.; Vacatello, M.; Corradini, P. *Polym. Commun*. **1989**, *30*, 16.

(2) Cavallo, L.; Guerra, G.; Corradini, P.; Resconi, L.; Waymouth, R. M. *Macromolecules* **1993**, *26*, 260.

(3) Guerra, G.; Cavallo, L.; Moscardi, G.; Vacatello, M.; Corradini, P. *J. Am. Chem. Soc.* **1994**, *116*, 2988.

(4) Hart, J. R.; Rappé, A. K. *J. Am. Chem. Soc.* **1993**, *115*, 6159.

(5) Cavallo, L.; Guerra, G. *Macromolecules* **1996**, *29*, 2729.

(6) (a) Woo, T. K.; Fan, L.; Ziegler, T. *Organometallics* **1994**, *13*, 2252. (b) Woo, T. K.; Fan, L.; Ziegler, T. *Organometallics* **1994**, *13*, 432. (c) Lohrenz, J. C. W.; Woo, T. K.; Ziegler, T. *J. Am. Chem. Soc.* **1995**, *117*, 12793. (d) Lohrenz, J. C. W.; Woo, T. K.; Fan, L.; Ziegler, T. *J. Organomet. Chem.* **1995**, *497*, 91. (e) Fan, L.; Krzywicki, A.; Somogyvari, A.; Ziegler, T. *Inorg. Chem.* **1994**, *33*, 5287. (f) Fan, L.; Harrison, D.; Deng, L.; Woo, T. K.; Swerhone, D.; Ziegler, T. *Can. J. Chem.* **1995**, *73*, 989. (g) Fan, L.; Krzywicki, A.; Somogyvari, A.; Ziegler, T. *Inorg. Chem.* **1996**, *25*, 4003. (h) Fan, L.; Harrison, D.; Woo, T. K.; Ziegler, T. *Organometallics* **1995**, *14*, 2018. (i) Deng, L.; Margl, P. M.; Ziegler, T. *J. Am. Chem. Soc.* **1997**, *119*, 1094. (j) Margl, P. M.; Ziegler, T. *J. Am. Chem. Soc.* **1996**, *118*, 7337. (k) Margl, P.; Ziegler, T. *Organometallics* **1996**, *15*, 5519. (l) Froese, R. D. J.; Musaev, D. G.; Morokuma, K. *J. Am. Chem. Soc.* **1997**, *119*, 7190.

(7) (a) Castonguay, L. A.; Rappé, A. K. *J. Am. Chem. Soc.* **1992**, *114*, 5832. (b) Kawamura-Kuribayashi, H.; Koga, N.; Morokuma, K. *J. Am. Chem. Soc.* **1992**, *114*, 8687. (c) Michalak, A.; Ziegler, T. *Organometallics* **1999**, *18*, 3998. (d) Hart, J. R.; Rappé, A. K. *J. Am. Chem. Soc.* **1993**, *115*, 6159. (e) Morokuma, K.; Yoshida, T.; Koga, N. *Organometallics* **1996**, *15*, 2766. (f) Strömberg, S.; Zetterberg, K.; Siegbahn, P. E. M. *J. Chem. Soc., Dalton Trans.* **1997**, 4147. (g) Lauher, J. W.; Hoffmann, R. *J. Am. Chem. Soc.* **1976**, *98*, 1729. (h) Gleiter, R.; Hyla-Kryspin, I.; Niu, S.; Erker, G. *Organometallics* **1993**, *12*, 3828. (i) Prosenc, M.-H.; Janiak, C.; Brintzinger, H.-H. *Organometallics* **1992**, *11*, 4036. (j) Kawamura-Kuribayashi, H.; Koga, N.; Morokuma, K. *J. Am. Chem. Soc.* **1992**, *114*, 2359. (k) Bierwagen, E. P.; Bercaw, J. E.; Goddard, W. A., III. *J. Am. Chem. Soc.* **1994**, *116*, 1481. (l) Weiss, H.; Ehrig, M.; Ahlrichs, R. *J. Am. Chem. Soc.* **1994**, *116*, 4919. (m) Das, P. K.; Dockter, D. W.; Fuhey, D. R.; Lauffer, D. E.; Hawkins, G. D.; Li, J.; Zhu, T.; Cramer, C. J.; Truhlar, D. G.; Dapprich, S.; Frose, R. D.; Holthausen, M. C.; Liu, Z.; Mogi, K.; Vyboischikov, S.; Musaev, D. G.; Morokuma, K. *ACS Symp. Ser.* **1999**, *721*, 208. (n) Bierwagen, E. P.; Bercaw, J. E.; Goddard, W. A., III. *J. Am. Chem. Soc.* **1994**, *116*, 1481. (o) Bernardi, F.; Bottoni, A.; Calcinari, M.; Rossi, I.; Robb, M. A. *J. Phys. Chem. A* **1997**, *101*, 6310. (p) Jensen, V. R.; Børve, K. J. *J. Comput. Chem.* **1998**, *19*, 947. (q) Margl, P.; Deng, L.; Ziegler, T. *Top. Catal.* **1999**, *7*, 187. (r) Margl, P.; Deng, L.; Ziegler, T. *J. Am. Chem. Soc.* **1998**, *120*, 5517. (s) Margl, P.; Deng, L.; Ziegler, T. *Organometallics* **1998**, *17*, 933. (t) Margl, P.; Deng, L.; Ziegler, T. *J. Am. Chem. Soc.* **1999**, *121*, 154. (u) Deng, L.; Ziegler, T.; Woo, T. K.; Margl, P.; Fan, L. *Organometallics* **1998**, *17*, 3240.

(8) (a) Woo, T. K.; Margl, P. M.; Lohrenz, J. C. W.; Blöchl, P. E.; Ziegler, T. *J. Am. Chem. Soc.* **1996**, *118*, 13021. (b) Woo, T. K.; Margl, P. M.; Blöchl, P. E.; Ziegler, T. *Organometallics* **1997**, *16*, 3454. (c) Woo, T. K.; Margl, P. M.; Deng, L.; Ziegler, T. *Catal. Today* **1999**, *50*, 479. (d) Margl, P. M.; Woo, T. K.; Blöchl, P. E.; Ziegler, T. *J. Am. Chem. Soc.* **1998**, *120*, 2174. (e) Margl, P.; Lohrenz, J. C. W.; Blöchl, P.; Ziegler, T. *J. Am. Chem. Soc.* **1996**, *118*, 4434. (f) Meier, R. J.; van Dormaele, G. H. J.; Larlori, S.; Buda, F. *J. Am. Chem. Soc.* **1994**, *116*, 7274. (g) Boero, M.; Parrinello, N.; Terakura, K. *J. Am. Chem. Soc.* **1998**, *120*, 2746.

(9) (a) Deng, L.; Woo, T. K.; Cavallo, L.; Margl, P. M.; Ziegler, T. *J. Am. Chem. Soc.* **1997**, *119*, 6177. (b) Woo, T. K.; Margl, P. M.; Blöchl, P. E.; Ziegler, T. *J. Phys. Chem. B* **1997**, *101*, 7877. (c) Musaev, D. G.; Froese, R. D. J.; Morokuma, K. *Organometallics* **1998**, *17*, 1850. (d) Deng, L.; Ziegler, T.; Woo, T. K.; Margl, P.; Fan, L. *Organometallics* **1998**, *17*, 3240.

(10) Brintzinger, H. H.; Fischer, D.; Mülhaupt, R.; Rieger, B.; Waymouth, R. M. *Angew. Chem., Int. Ed. Engl.* **1995**, *34*, 1143.

(11) (a) Johnson, L. K.; Killian, C. M.; Brookhart, M. *J. Am. Chem. Soc.* **1995**, *117*, 6414. (b) Johnson, L. K.; Mecking, S.; Brookhart, M. *J. Am. Chem. Soc.* **1996**, *118*, 267.

(12) Searle, M. S.; Westwell, M. S.; Williams, D. H. *J. Chem. Soc., Perkin Trans.* **1995**, *2*, 141.

(13) Woo, T. K.; Ziegler, T. *J. Organomet. Chem.*, in press.
(14) In general the corrections are found to be near the entropic limit of approximately 13 kcal/mol at 300 K. See also refs 6c and 9c.
(15) Beveridge, D. L.; DiCapua, F. M. *Annu. Rev. Biophys. Chem.* **1989**, *18*, 431.
(16) Searle, M. S.; Williams, D. H. *J. Am. Chem. Soc.* **1992**, *114*, 10690.
(17) (a) Baerends, E. J.; Ellis, D. E.; Ros, P. *Chem. Phys.* **1973**, *2*, 41. (b) Baerends, E. J.; Ros, P. *Chem. Phys.* **1973**, *2*, 52. (c) Baerends, E. J. Ph.D. Thesis, Free University, Amsterdam, The Netherlands, 1975. (d) Velde, G. te; Baerends, E. J. *J. Comput. Chem.* **1992**, *99*, 84.
(18) (a) Snijders, J. G.; Baerends, E. J.; Vernoijs, P. *At. Data Nucl. Data Tables* **1982**, *26*, 483. (b) Vernoijs, P.; Snijders, J. G.; Baerends, E. J. *Slater Type Basis Functions for the Whole Periodic System*; Department of Theoretical Chemistry, Free University: Amsterdam, The Netherlands, 1981. (c) Krijn, J.; Baerends, E. J. *Fit Functions in the HFS Method*; Department of Theoretical Chemistry, Free University: Amsterdam, The Netherlands, 1984.
(19) Vosko, S. H.; Wilk, L.; Nusair, M. *Can. J. Phys.* **1980**, *58*, 1200.
(20) Becke, A. *Phys. Rev. A* **1988**, *38*, 3098.
(21) (a) Perdew, J. P. *Phys. Rev. B* **1986**, *34*, 7406. (b) Perdew, J. P. *Phys. Rev. B* **1986**, *33*, 8822.
(22) (a) Snijders, J. G.; Baerends, E. J. *Mol. Phys.* **1978**, *36*, 1789. (b) Snijders, J. G.; Baerends, E. J.; Ros, P. *Mol. Phys.* **1979**, *38*, 1909.
(23) (a) Woo, T. K.; Cavallo, L.; Ziegler, T. *Theor. Chim. Acta* **1998**, *100*, 307. (b) Woo, T. K. Ph.D. Thesis, University of Calgary, Canada, 1998.
(24) Maseras, F.; Morokuma, K. *J. Comput. Chem.* **1995**, *16*, 1170.
(25) (a) Sinnema, J. C. M.; Frendesak, G. H. B.; tom-Dieck, H. *J. Organomet. Chem.* **1990**, *390*, 237. (b) Diercks, R.; Kopf, J.; tom-Dieck, H. *Acta Crystallogr., Sect. C* **1984**, *40*, 363. (c) van-Asselt, R.; Elsevier: C. J.; Smeets, W. J. J.; Spek, A. L. *Inorg. Chem.* **1994**, *33*, 1521.
(26) Cornell, W. D.; Cieplak, P.; Bayly, C. I.; Gould, I. R.; Merz, K. M., Jr.; Ferguson, D. M.; Spellmeyer, D. C.; Fox, T.; Caldwell, J. W.; Kollman, P. A. *J. Am. Chem. Soc.* **1995**, *117*, 5179.
(27) Rappé, A. K.; Casewit, C. J.; Colwell, K. S.; Goddard, W. A., III; Skiff, W. M. *J. Am. Chem. Soc.* **1992**, *114*, 10024.
(28) (a) Hehre, W. J.; Radom, L.; Schleyer, P. v. R.; Pople, J. A. *Ab Initio Molecular Orbital Theory*; John Wiley & Sons: New York, 1986. (b) McQuarrie, D. A. *Statistical Thermodynamics*; Harper & Row: New York, 1973.
(29) Car, R.; Parrinello, M. *Phys. Rev. Lett.* **1985**, *55*, 2471.
(30) Blöchl, P. E. *Phys. Rev. B* **1994**, *50*, 17953.
(31) (a) Dunitz, J. D. *Chem. Biol.* **1995**, *2*, 709. (b) Dunitz, J. D. *Science* **1994**, *264*, 670.
(32) Finkelstein, A. V.; Janin, J. *Protein Eng.* **1989**, *3*, 1.
(33) The equipartition of energy theorem states that all degrees of freedom contribute $RT/2$ to the ethalpy. Since the energy levels in our classical molecular dynamics simulation are continuous, there is no change in the sum of ΔH_{vib}, ΔH_{trans}, and ΔH_{rot} throughout the slow growth simulation.
(34) Unfortunately, constrained QM/MM frequency calculations at the capture transition states of **2** and **3** could not be performed. Therefore, we have not estimated the free energy barrier of capture from frequency calcultions of models **2** and **3**.
(35) The exception here is that the multiple time step procedure was not applied.
(36) With mass rescaling the ficticious time scale is equivalent to approximately 1.5 ps.
(37) Rix, F.; Brookhart, M. *J. Am. Chem. Soc.* **1995**, *117*, 1137.
(38) Klamt, A.; Schuurmann, G. *J. Chem. Soc., Perkin Trans.* **1993**, *2*, 799.
(39) Pye, C.; Zielger, T. *Theor. Chem. Acc.* **1999**, *101*, 396.
(40) COSMO calculations have been performed on the pure QM model **1**, using the gas-phase optimized structures of the π-complex, ethene and the metal alkyl complexes. Since, the cavitation free energy has not been considered, the value given (2.7 kcal/mol) is a high estimate.
(41) Ben-Naim, A. *Solvation Thermodynamics*; Plenum Press: New York, 1987.